JPhys Materials

TECHNICAL NOTE • OPEN ACCESS

Fabrication and characterization of large-area suspended $MoSe_2$ crystals down to the monolayer

To cite this article: Sebin Varghese *et al* 2021 *J. Phys. Mater.* **4** 046001

IOP Publishing J. Phys. Mater. 4 (2021) 046001 https://doi.org/10.1088/2515-7639/ac2060

Journal of Physics: Materials

OPEN ACCESS

RECEIVED
2 July 2021

REVISED
6 August 2021

ACCEPTED FOR PUBLICATION
24 August 2021

PUBLISHED
7 September 2021

TECHNICAL NOTE

Fabrication and characterization of large-area suspended $MoSe_2$ crystals down to the monolayer

Sebin Varghese[1,3], David Saleta Reig[1,3], Jake Dudley Mehew[1], Alexander Block[1], Alexandros El Sachat[1], Emigdio Chávez-Ángel[1], Marianna Sledzinska[1], Belén Ballesteros[1], Clivia M Sotomayor Torres[1,2] and Klaas-Jan Tielrooij[1,*]

[1] Catalan Institute of Nanoscience and Nanotechnology (ICN2), BIST and CSIC, Campus UAB, Bellaterra, 08193 Barcelona, Spain
[2] ICREA, Pg. Lluís Companys 23, 08010 Barcelona, Spain
[3] Equal contributions
[*] Author to whom any correspondence should be addressed.

E-mail: klaas.tielrooij@icn2.cat

Keywords: suspended flakes, transition metal dichalcogenides, $MoSe_2$, dry-transfer, optical absorption

Supplementary material for this article is available online

Abstract

Many layered materials, such as graphene and transition metal dichalcogenides, can be exfoliated down to atomic or molecular monolayers. These materials exhibit exciting material properties that can be exploited for several promising device concepts. Thinner materials lead to an increased surface-to-volume ratio, with mono- and bi-layers being basically pure surfaces. Thin crystals containing more than two layers also often behave as an all-surface material, depending on the physical property of interest. As a result, flakes of layered materials are typically highly sensitive to their environment, which is undesirable for a broad range of studies and potential devices. Material systems based on suspended flakes overcome this issue, yet often require complex fabrication procedures. Here, we demonstrate the relatively straightforward fabrication of exfoliated $MoSe_2$ flakes down to the monolayer, suspended over unprecedentedly large holes with a diameter of 15 μm. We describe our fabrication methods in detail, present characterization measurements of the fabricated structures, and, finally, exploit these suspended flakes for accurate optical absorption measurements.

1. Introduction

Flakes of layered materials are often sensitive to their environment through proximity effects and other coupling mechanisms, such as long-range Coulomb scattering [1, 2], dielectric effects [3, 4], phonon scattering [5, 6], and near-field energy transfer [7]. These interactions affect the electrical, optical, thermal and mechanical properties of flakes placed on (underneath) a substrate (superstrate). For a broad range of applications and scientific studies it is essential to avoid these effects induced by a material's environment. This can be achieved by using freely suspended crystals, such as flakes placed on holes or trenches. Suspended systems are interesting because of their electrical, optical, thermal and mechanical properties (see figure 1), and often exhibit improved figures of merit. Reduced scattering with environmental charges, for example, can lead to an increased charge mobility [8, 9]. Furthermore, the optical absorption or emission is not affected by the dielectric environment of the suspended material, and therefore reflects the intrinsic properties of the isolated material [10, 11]. Moreover, without substrates and superstrates there is no material that can act as a heat sink, such that the intrinsic thermal properties of the material are obtained [12, 13]. Finally, the same holds for mechanical properties, where no substrate properties have to be taken into account [14, 15]. Indeed, potential applications are being explored, where micro- and nano-electromechanical systems, and force and mass sensing systems [16], among others, exploit suspended materials.

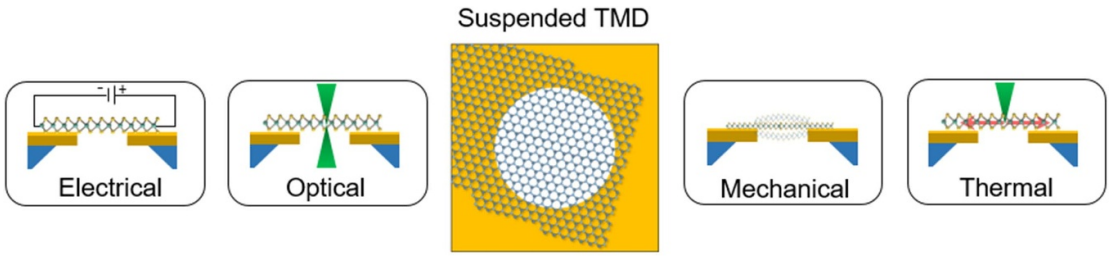

Figure 1. Schematic illustration of a suspended flake (center) and the opportunities this material system offers in terms of electrical, optical, mechanical and thermal studies.

Table 1. Summary of suspended TMD systems prepared from exfoliated material.

Material	Thickness	Substrate	Hole size	Transfer method	Reference
MoS_2	1 layer	SiO_2/Si	5 μm	PMMA	[49]
	1 layer	Si_3N_4	1.2 μm	PMMA	[50]
	1 layer	Si	2 or 5 μm	PMMA	[51]
	1 layer	SiO_2/Si	550 nm	PMMA	[52]
	1, 2 layers	Au	4 μm	PMMA	[43]
	1–10 layers	Au/Ti	4 μm		[53]
WSe_2	1 layer	SiO_2/Si	2−5 μm		[54]
	1–3 layers	SiO_2/Si	1.5 μm		[55]
	4, 6 layers	Si_3N_4	5 μm	PMMA	[56]
	5, 6, 12, 14 layers	SiO_2/Si	1.55 or 2.6 μm	Dry transfer	[57]
WS_2	13–107 nm	Si	10 μm	Dry transfer	[58]
$MoSe_2$	1–5, 7, 70 layers	Au	15 μm	Dry transfer	This work
	3–9 layers, bulk	Au	15 μm	Dry transfer	[15]
	1, 2 layers	Au	2.5 μm	PMMA	[43]
	5–80 nm	Si	10 μm	Dry transfer	[59]
	45–140 nm	Si	22 × 22 μm	Dry transfer	[60]

Impressive material systems have been fabricated with suspended graphene flakes [17–19], suspended transition metal dichalcogenides (TMDs) [20, 21] and suspended Van der Waals heterostructures [22, 23], where exfoliated flakes are typically suspended over a few μm. For several studies and applications—especially those focusing on optical, optoelectronic, thermal and mechanical properties—a larger suspended area is desirable, or, in some cases, crucial. We note that large-area suspended material systems can be prepared using crystals grown by chemical vapor deposition, rather than exfoliated flakes. Such systems are typically limited to monolayers. Exfoliated flakes do not suffer this limitation. However they are often suspended over a well or trench, rather than over a hole that goes completely through the substrate. Furthermore, the suspended flakes should ideally be monocrystalline, free of residues, free of strain, relatively easy to fabricate, and durable. Here, we demonstrate the fabrication of such systems using polydimethylsiloxane (PDMS)-assisted dry transfer, based on the method described in [24], onto a carefully prepared substrate with a 15 μm diameter hole with a full transmission window. We demonstrate the ability to fabricate these material systems with flakes down to the monolayer. To the best of our knowledge, these are the largest, suspended, TMD monolayer flakes based on exfoliated material, that have been fabricated to date (see table 1). Furthermore, with sufficiently high quality of exfoliated flakes, even larger suspended areas are likely attainable with our method. We characterize the suspended flakes using a variety of techniques, and perform experiments, where we obtain the optical absorption of $MoSe_2$ flakes as a function of flake thickness.

2. Method

We fabricate free-standing TMD flakes by exfoliation onto a viscoelastic PDMS stamp, followed by dry-transfer onto a substrate with a pre-fabricated hole. PDMS-assisted dry transfer is a commonly applied method that involves no wet chemistry or capillary forces, thus leading to relatively clean surfaces. As a substrate, we use commercial Si_3N_4 membranes with a single 15 μm hole (Norcada, NTPR005D-C15) and, crucially, metalize their surface with titanium (5 nm) and gold (50 nm). Metal-coating the substrates prior to transfer significantly enhances the transfer yield thanks to the strong adhesion between gold and chalcogen

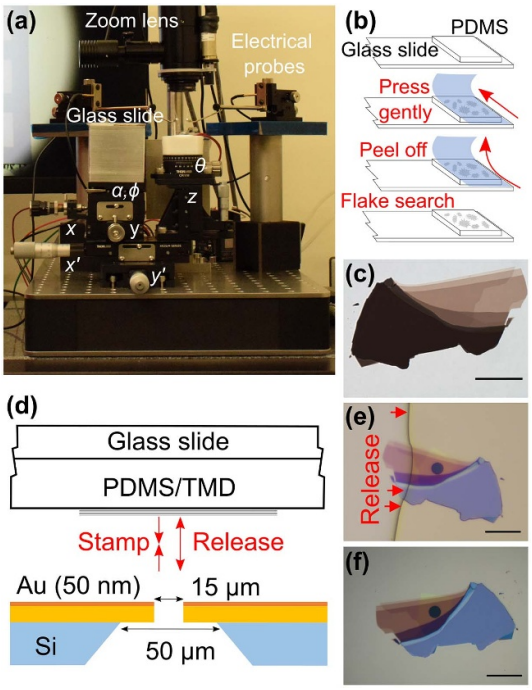

Figure 2. (a) Home-built transfer stage/probe station setup. (b) Scheme of the exfoliation method on PDMS. (c) Exfoliated flake on PDMS in transmission microscopy. (d) Schematics of the stamping process. (e) Flake being released on Au-coated Si_3N_4 holey chip, and (f) optical microscope image of completely transferred flake. Scale bars in (c)–(f) correspond to 50 μm.

atoms [25]. The exfoliation and transfer is based on the method of [26], while our home-built dry-transfer setup, shown in figure 2(a), is a modified version based on the design from [24]. Below, we describe the fabrication process in detail.

For exfoliation, we sandwich a flat piece of TMD material between two strips of Scotch tape. The crystal is thinned down and spread over an area of ~1 × 2 cm^2 by bringing the two tapes in contact a few times at different, yet close, positions. We use both these strips as parent tapes, from which we produce 'exfoliation tapes' by peeling the thin crystals with a fresh piece of Scotch tape. We immediately bring the 'exfoliation tapes' in contact with a PDMS bed, placed on the edge of a fresh glass slide, as shown in figure 2(b). Rubbing gently with a cotton swab typically ensures good contact between the crystals and PDMS, thus producing larger flakes. Additionally, fast peeling of the exfoliation tapes increases the yield and area of thin flakes. We perform the flake search under an optical microscope (see image in figure 2(c)) in both transmission and reflection configurations to identify wrinkle-free, large and thickness-homogeneous flakes with sharp edges, indicating high quality and single-crystalline nature. We select flakes with the desired thickness using calibrated optical contrast measurements.

For the preparation of the PDMS stamp, we mix silicone elastomer curing agent and silicone elastomer base (SYLGARD 184) in 1:10 wt% proportions. We stir the mixture and place it in a vacuum desiccator to force the release of air bubbles until it appears transparent, which is a subtle step that we identified as crucial. We then spread the mixture in a Petri dish in order to achieve a bubble-free, homogeneous ~1 mm thick PDMS film with a smooth surface. The closed Petri dish is left drying for ~48 h in air and later sealed to avoid dust and loss of stickiness. Finally, we cut the PDMS in appropriately sized pieces at the moment of use, selecting PDMS from the center of the Petri dish, where it has the highest flatness.

For the deterministic, precise transfer of flakes, we use a home-built dry-transfer stage inspired by the design of [24]. The most important improvements that we have implemented are the following. First, we improved the mechanical stability of the imaging part of the stage by using a vertical support post with increased mass, and by equipping the stage with motorized zoom and focus. Second, we included a vacuum chuck that allows the gentle mounting and dismounting of substrates and samples, with integrated temperature control. Third, we equipped the transfer stage with six degrees of freedom to align the flake with respect to the target substrate (x, y, z, rotation θ, pitch α and roll ϕ), see figure 2(a). The tilt degrees of freedom allow for precise control of the flake-substrate contact angle and the direction in which the flake will be released, which is crucial for preparing suspended flakes. In addition, we use x' and y' stages at the base of the setup that conveniently allow for sample inspection without loss of alignment between flake and

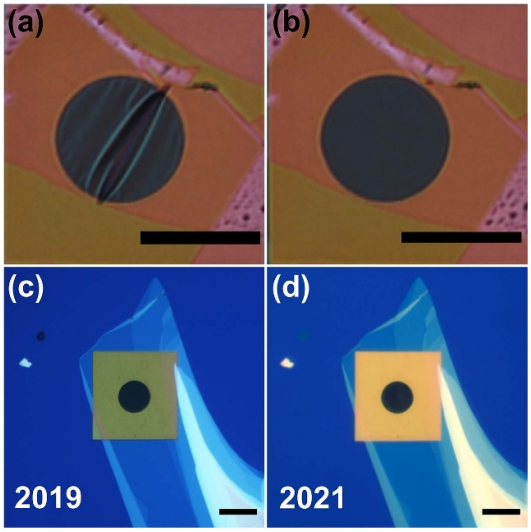

Figure 3. (a) Wrinkled suspended region of a $MoSe_2$ sample which is (b) flattened by 'ironing': heating at 150 °C for 30 min. Optical microscope images of a suspended bilayer $MoSe_2$ sample (c) directly after fabrication and (d) almost two years later. All scale bars are 20 μm.

substrate. Last, we included probe-station functionalities for electrical characterization of 2D materials and devices. For this, we added electrical probes mounted on micromanipulators that are placed on elevated platforms around the working area. The supporting information (available online at stacks.iop.org/JPMATER/4/046001/mmedia) provides a detailed description of the components needed to assemble our modified setup for the transfer of 2D materials.

In order to transfer a flake onto a gold-coated holey substrate, we use the z-stage to bring the substrate toward the viscoelastic PDMS stamp supporting the flake of interest, as schematically depicted in figure 2(d). Prior to stamping, we align the flake over the hole of the target substrate and adjust the α- and ϕ-stages to define the contact and release directions. We obtain the highest yield, when the flake is released onto the substrate starting from the thinner and sharper edge of the flake toward thicker or less ideal regions, see figure 2(e) as an example. The flake is being released if the optical contrast of the flake on both sides of the PDMS-flake contact interface is similar. If not, this indicates that the flake is still on PDMS. A PDMS-flake contact interface that is not straight means that the flake has more affinity to either substrate or PDMS. In the exemplary transfer of figure 2(e), the flake sticks better to Au and the retracting PDMS-flake contact interface moves faster on the flake than on gold, thus simplifying the transfer. The reason for this is a low adhesion energy for TMDs to PDMS (18 mJ m^{-2} for MoS_2) [27] compared to that for TMDs to gold (1207.26 mJ m^{-2} for MoS_2) [28]. The most critical step comes at the moment of releasing the flake in the suspended region, where the PDMS-flake contact interface moves very slowly, because the flake is more inclined to stay supported on PDMS rather than suspended in air. We control this critical step by using an extremely slow release, and achieving a straight PDMS contact interface. The optical microscope image in figure 2(f) shows an example of a transferred $MoSe_2$ flake. With this technique, we have achieved the successful fabrication of various mono-, bilayer and thicker suspended TMD flakes over large-areas (177 μm^2).

We note that in some cases, the fabrication of suspended flakes results in wrinkled flakes due to significant straining during dry-transfer and/or relative changes in ambient conditions (see figure 3(a)). Interestingly, we found that we can easily remove such wrinkles by an annealing step at 150 °C for ~30 min. This 'ironing' of suspended TMD flakes is shown figure 3(b). Here, we show a $MoSe_2$ flake before and after being 'ironed', which can be conveniently performed immediately after transfer on the heating stage. In some cases, flat flakes wrinkle due to relative changes in temperature or humidity and can later be flattened on a hot plate. Importantly, we show that our suspended $MoSe_2$ flakes are highly stable. Figures 3(c) and (d) show exemplary images of a suspended bilayer $MoSe_2$, directly after preparation in 2019, and almost two years later in 2021, respectively. There is no visible degradation. We have found that there is also no significant degradation for photoluminescence (PL) measurements, which show the same number of counts (within 2%), PL peak position (within 0.2%) and PL linewidth (within 0.4%) for measurements taken 9 months apart.

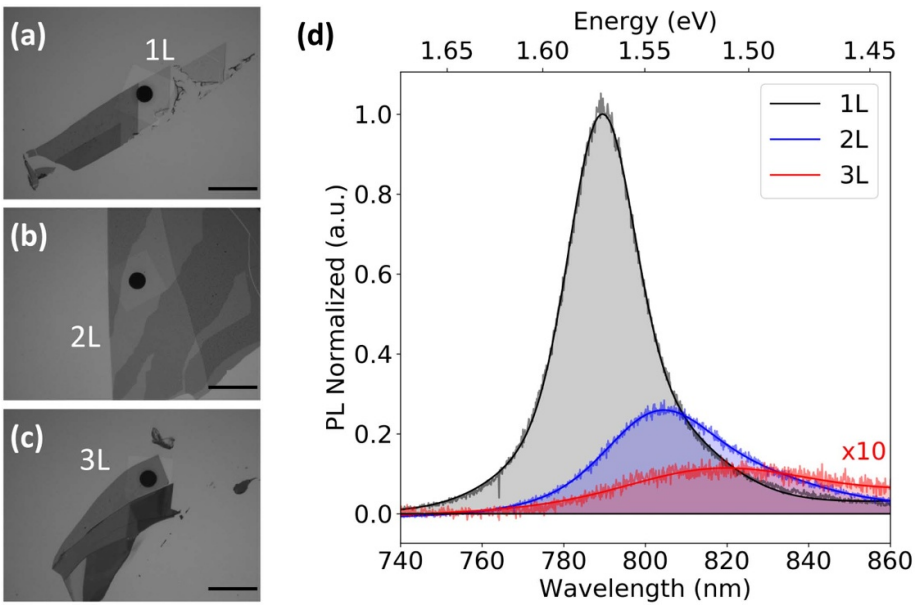

Figure 4. (a)–(c) Optical images of dry-transferred (a) mono-, (b) bi-, and (c) trilayer $MoSe_2$ flakes over 15 μm holes. (d) PL spectra corresponding to the suspended region of these flakes. Scale bars are 50 μm.

3. Results

3.1. Characterization of large-area suspended flakes

We will now show measurement results obtained using thin TMD flakes suspended over 15 μm holes, i.e. suspended over an area of 177 μm^2. Although we have prepared suspended flakes using various TMD materials, we now focus on $MoSe_2$. The thickness of the prepared flakes varies between 1 layer (1L) and ~70 layers (70L). We show optical microscope images of suspended $MoSe_2$ flakes with a thickness of 1, 2 and 3 layers in figures 4(a)–(c). We performed PL spectroscopy measurements on these suspended $MoSe_2$ flakes, in order to confirm their thickness. We use a CW laser with a wavelength of 532 nm to excite the center of the suspended flake. The PL emission is collected, dispersed with a grating-spectrometer, and detected by a nitrogen-cooled CCD. Figure 4(d) shows the PL intensity of the suspended flakes shown in panels (a, b, c), normalized to the monolayer intensity. Our PL studies on monolayer $MoSe_2$ show a relatively intense emission peak centered at 790 nm (1.57 eV), in agreement with the exciton peak of monolayer $MoSe_2$ found in references [29, 30]. The PL spectrum of a bilayer $MoSe_2$ flake shows reduced intensity and the emission peak is red-shifted toward 805 nm (1.55 eV) compared to the monolayer. For a trilayer flake, the PL emission peak further red-shifts, broadens and the intensity drops significantly, also in agreement with observations in the literature [31, 32].

We further characterize our $MoSe_2$ samples using high-resolution transmission electron microscopy (HR-TEM). The HR-TEM images were collected at 80 kV in an ARM-200f (JEOL), as part of a previous work [15]. Such images, shown in figures 5(a) and (b), provide important information about the structure and quality of our suspended $MoSe_2$ flakes. From figure 5(a), the flake appears to be defect- and/or dislocation-free over tens of nm. The high-magnification TEM image in figure 5(b) depicts a honeycomb arrangement of atoms, indicating the single-crystalline structure with an interplanar distance ~0.28 nm, in perfect agreement with the literature [33]. The fast Fourier transform (FFT) pattern in figure 5(c) displays hexagonal symmetrical patterns, indicating the hexagonal lattice structure of the $MoSe_2$ single-crystals. Thus, we conclude that our flakes are highly crystalline.

In order to quantify the roughness and surface quality of our samples we performed atomic force microscopy (AFM) imaging in tapping mode. Figure 6(a) shows the 3D topography AFM image of a suspended bilayer $MoSe_2$ flake at the hole edge. Interestingly, we observe an abrupt sagging of the membrane at the edge of the suspended region of the sample. Similar effects were reported previously [34], and come from the exceptional ability of atomically thin materials to accommodate to the nano/microstructures of the substrate underneath [35]. Therefore, it is not surprising that the flake shows roughness on the supported region, as it is susceptible to the substrate's roughness. The RMS roughness (Rq) of the flake in the supported region (see figure 6(b)) is 2.8 ± 1.0 nm, which corresponds to the roughness of the metal-coated substrate.

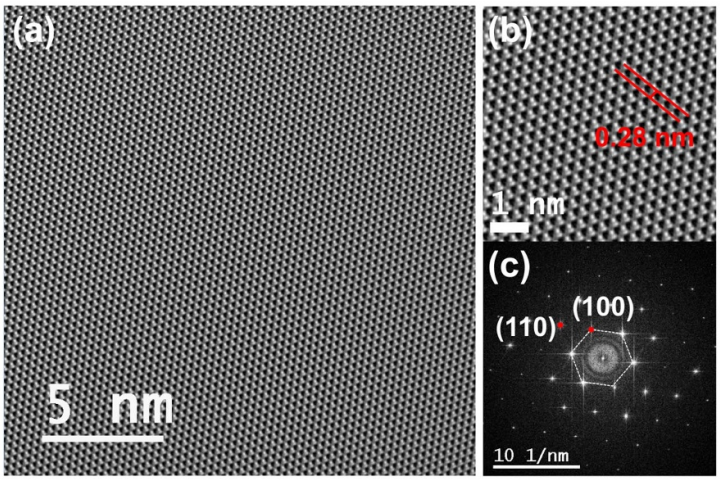

Figure 5. (a), (b) High-resolution TEM images of an exemplary suspended $MoSe_2$ flake. (c) FFT of the TEM image displaying hexagonal symmetrical patterns of $MoSe_2$.

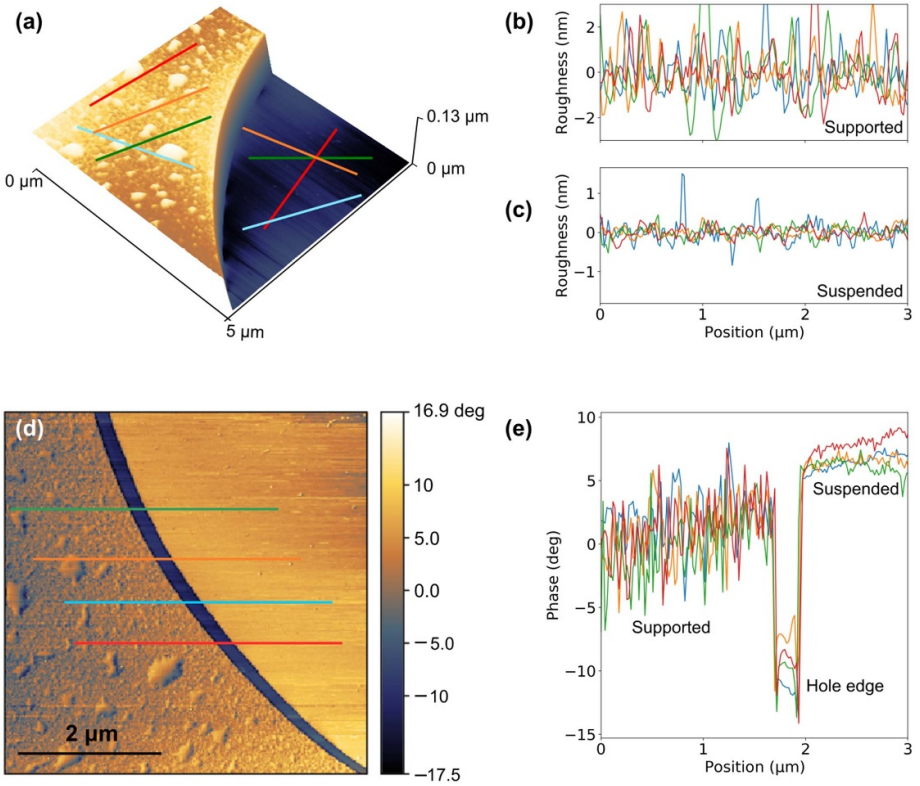

Figure 6. (a) AFM 3D topography image of the supported and suspended regions of a bilayer $MoSe_2$ sample and (b), (c) their corresponding roughness profiles. (d) AFM phase contrast image and (e) the phase profiles across different sample positions.

However, in the suspended region (see figure 6(c)), the surface quality is significantly higher: we find an Rq of 0.75 ± 0.25 nm over a 2×2 μm^2 area. This is similar to the thickness of a molecular monolayer (~0.7 nm), which suggests that the flake is atomically flat. The sub-nanometer roughness over several micrometers further demonstrates the absence of small wrinkles on the suspended region. Figures 6(d) and (e) shows the AFM phase contrast image and the profiles taken across different positions on the sample. The smooth phase signal in the suspended region shows uniform surface stiffness and adhesion between the AFM tip and surface, thus suggesting a homogeneous flake with undetectable levels of residues.

Another important aspect of these material systems is the quality of their chemical composition, which we address using energy-dispersive x-ray spectroscopy (EDX). Figure 7 shows the results for bilayer $MoSe_2$

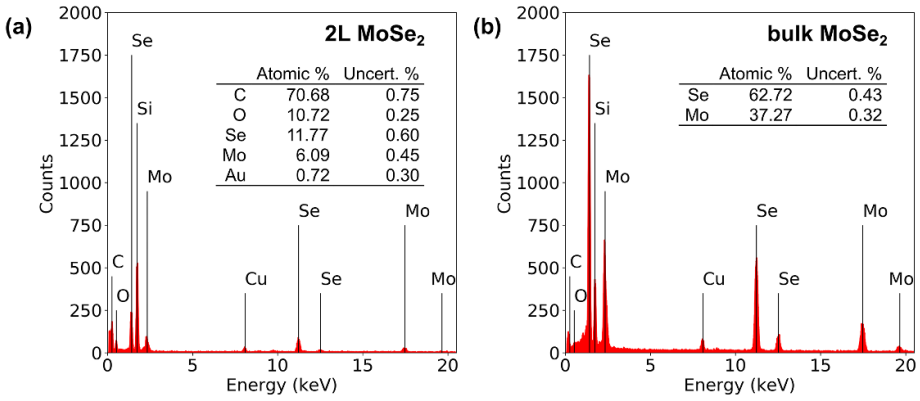

Figure 7. EDX spectra of suspended (a) bilayer and (b) bulk $MoSe_2$ flakes.

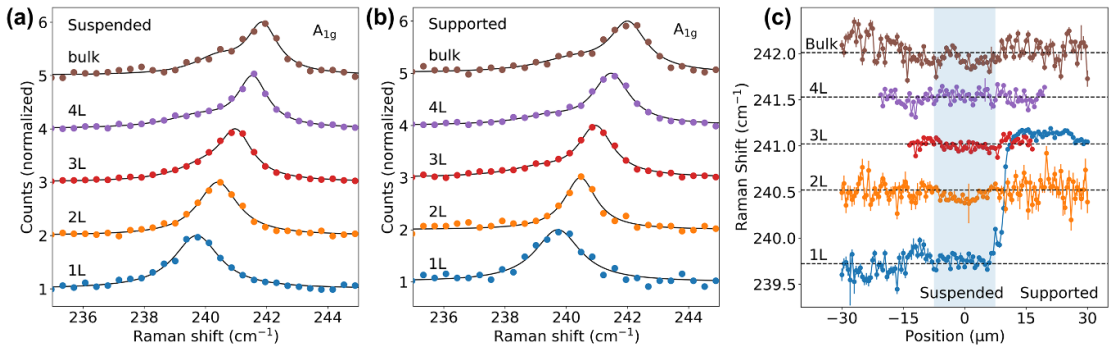

Figure 8. Raman spectra of (a) suspended and (b) supported $MoSe_2$ flakes of different thicknesses taken at 532 nm excitation wavelength. The solid lines are Lorentzian fits to the data. (c) Peak position of A_{1g} mode across suspended $MoSe_2$ flakes of 1–4 layers and bulk taken at 3 μW incident power at sample plane. The blue shaded area represents the suspended regions. The abrupt increase in peak position for the monolayer sample corresponds to a transition from 1 to 3 layers along the scan direction.

and a $MoSe_2$ flake with a thickness of ~50 nm. We find a decent ratio between Mo and Se, and relatively low traces of other elements, in particular for the thicker flake. This shows that our fabrication technique leads to suspended flakes with a very small amount of residues. We note that the bilayer sample shows a significant amount of C contamination, which we ascribe to deposition from the environment during the >1 year between sample preparation and performance of the EDX measurements. The thicker sample was significantly more fresh, and shows very little carbon contamination.

We also characterize the suspended $MoSe_2$ flakes by Raman scattering with a spectral resolution of 0.25 cm^{-1}, in order to extract information about strain in the suspended flake. The relative shifts in peak position of different Raman modes also provide information about the thickness of TMDs [36–38]. We use the same setup that we used for the PL measurements, and study the occurrence of strain-induced changes in the Raman spectra of our suspended and supported $MoSe_2$ flakes. Figures 8(a) and (b) show the A_{1g} mode for $MoSe_2$ flakes with thicknesses in the range 1–4 layers, and bulk. The results for supported and suspended $MoSe_2$ are very similar. For bulk $MoSe_2$, the A_{1g} peak position is located at 242 cm^{-1}, in agreement with previously reported values [39, 40]. The A_{1g} mode shifts to lower frequency upon reducing the flake thickness, and reaches a value of 239.7 cm^{-1} for monolayer $MoSe_2$, also consistent with results in the literature [30, 41]. The Raman measurements thus confirm the flake thicknesses we extracted from PL measurements.

In order to investigate strain, we take Raman spectra at different sample positions, and extract the peak position of the A_{1g} mode of $MoSe_2$ as a function of sample position (see figure 8(c)). We used very low incident power (3 μW at the sample plane) to avoid temperature-induced Raman shifts. The frequency of the A_{1g} mode barely varies in the suspended region of the sample, while it fluctuates in the supported part of the sample. These fluctuations are within, or very close to, the resolution limit of the spectrometer. Thus we conclude that there are no signs of strain-induced shifts within the suspended region (blue-shaded area in figure 8(c)).

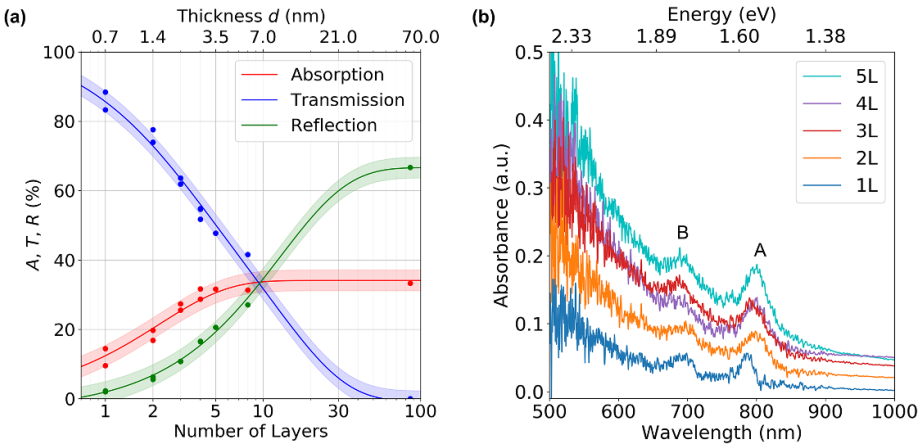

Figure 9. (a) Measured reflection R and transmission T values, together with the calculated absorption $A = 1 - R - T$ for suspended $MoSe_2$ flakes (532 nm) as a function of thickness. The solid lines and shaded regions represent a guide to the eye. (b) Spectra in the visible and NIR range acquired for 1–5 layers suspended $MoSe_2$ flakes.

3.2 Optical absorption measurements

We now present optical absorption measurements for $MoSe_2$, enabled by our exfoliated, few-layer, large-area, suspended, single-crystalline, unstrained, clean flakes. We first perform a systematic study of the optical absorption at 532 nm as a function of flake thickness in ambient conditions. We benefit from the fact that our holey substrates are open windows, suitable for transmission measurements, where light only interacts with the flake. We readily isolate the absorption of the flake by measuring the transmitted P_{trans} and reflected P_{refl} laser power, with respect to the incident power P_{inc}, using a calibrated power head (Thorlabs, S130 C) and a pristine substrate as reference. We obtain the optical absorbance A of the suspended flake from the following relation: $A = 1 - T - R = 1 - P_{trans}/P_{inc} - P_{refl}/P_{inc}$. Figure 9(a) shows the resulting absorption A, transmittance T and reflectance R values of the $MoSe_2$ flakes as a function of number of layers. We observe that the absorption increases with thickness and saturates quickly after 5 layers (5L). The material becomes quite strongly reflective as the number of layers increases toward the bulk. We measured multiple samples in the 1–3 layer regime, and obtained very reproducible R values of $2 \pm 0.2\%$ and $6 \pm 0.2\%$ for 1 and 2 layers, respectively, showing minimal sample-to-sample variations. The reflectivity of TMDs has also been shown to effectively reveal the thickness of each flake [42], which we find to increase from 2% to 20% from 1 to 5 layers. For the monolayer and bulk $MoSe_2$, we obtained an absorption of $10 \pm 3\%$ and $33 \pm 3\%$, respectively. We note that for thicker flakes, internal reflections inside the material can occur, giving rise to non-monotonous behavior of the optical properties as a function of thickness.

Available absorption values for mono- and few-layer TMDs in the literature are scarce and scattered. For monolayer $MoSe_2$ supported on SiO_2/Si, an absorption of $23 \pm 8\%$ was estimated for a wavelength of 514 nm [30]. Others have determined values of 5.6% and 9.7% for light at 633 nm for suspended monolayer and bilayer $MoSe_2$ [43], respectively. We note that most of the values found in the literature are obtained either on supported flakes or flakes suspended over small holes with sizes comparable to the laser spot, or shallow, well-like holes. In these cases, the absorption is calculated using an analysis that relies on knowledge of the complex permittivities of materials in the sample, which introduces potential errors in the obtained absorption values. In contrast, our large-area suspended flakes allow for more direct optical absorption measurements that do not require knowledge of any dielectric properties of the substrate.

The second optical absorption experiment we perform is in the range from 500 to 1000 nm using a commercial UV–Vis spectrometer (Hyperion 2000, Bruker). Figure 9(b) shows the absorption spectra in the Vis to near-infrared range for 1–5 layers suspended $MoSe_2$ flakes. Absorption and excitonic features for bulk TMD crystals are well known since they have been studied since several decades [44, 45]. We find exciton peaks around 800 nm (A-peak) and 700 nm (B-peak), in agreement with previous studies on $MoSe_2$ [30, 46]. We also observe that the A-exciton peak exhibits a sudden blue-shift at the monolayer thickness, similar to early findings in TMDs [47, 48]. The energy difference between the A and B peaks, which is an indication of the strength of spin-orbit interaction, is ~220 meV for $MoSe_2$, in agreement with the literature [31, 48]. This shows that we can use our large-area, clean, suspended flakes for both quantitative absorption measurements at a single wavelength, and spectrally resolved absorption measurements.

As a final demonstration of the usefulness of suspended crystals, we compare PL measurements on supported and suspended regions of mono-, bi-, and trilayer $MoSe_2$ flakes. We clearly observe that

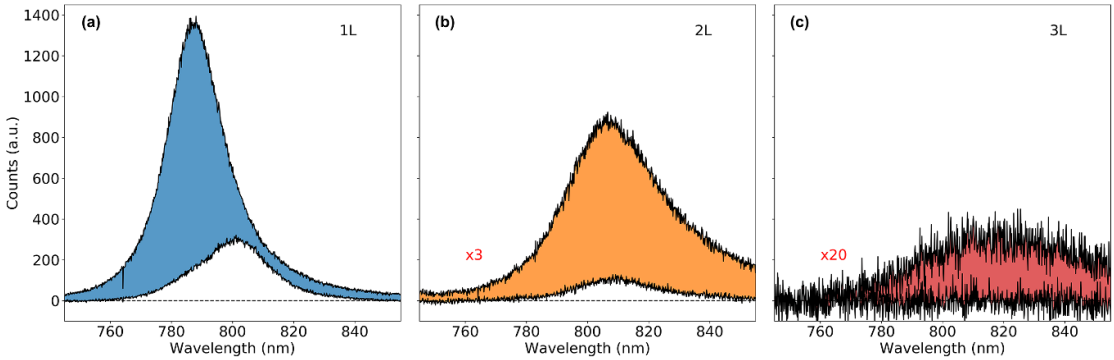

Figure 10. PL emission from (a) 1L, (b) 2L, and (c) 3L $MoSe_2$ flakes as measured on supported and suspended regions around one year after their fabrication. The shaded areas represent the PL enhancement on the suspended regions. Data sets presented in panels (b) and (c) are scaled by a factor 3 and 20, respectively.

suspended TMDs result in brighter emission, in agreement with the results of [43]. The PL signal of the trilayer $MoSe_2$ flake is only detectable in the suspended regions. Moreover, we performed these PL measurements on samples that were more than one year old, which also confirms that their optical properties do not significantly degrade over time. These results demonstrate an exceptional quality and stability of the suspended flakes used in this work.

4. Conclusion

In summary, we have developed a fabrication procedure to obtain large-area, suspended TMD flakes, based on standard PDMS-assisted dry-transfer, combined with gold-coated, commercial substrates with 15 μm-diameter holes. We have prepared a set of suspended $MoSe_2$ sample ranging from monolayer to 70 layers. Careful characterization of the suspended flakes using PL, AFM, TEM, EDX, and Raman scattering measurements shows that they are single-crystalline, clean, and unstrained. We also found that the wrinkles on the suspended region can be removed through thermal annealing, and that samples do not degrade during a time period of $>$20 months. Finally, we showed two optical absorption experiments performed on the suspended $MoSe_2$ flakes, which are exempt from any artefacts or errors induced by their environment. Beyond optical measurements, we envision broad use of our suspended TMD structures for electrical, thermal and mechanical studies and potential applications requiring an isolated response from environment-free thin flakes, in addition to applications and studies requiring photon emission with minimal losses.

Data availability statement

The data that support the findings of this study are available upon reasonable request from the authors.

Acknowledgments

The authors would like to thank Emerson Coy (CNBM-AMU) for sharing the HR-TEM images. S V and D S R acknowledge the support of the Spanish Ministry of Economy through FPI-SO 2018 and FPI-SO 2019, respectively. ICN2 was supported by the Severo Ochoa program from Spanish MINECO (Grant No. SEV-2017-0706). K J T acknowledges funding from the European Union's Horizon 2020 research and innovation program under Grant Agreement No. 804349 (ERC StG CUHL), RyC Fellowship No. RYC-2017-22330, and IAE Project PID2019-111673GB-I00. A E S, E C A, M S and C M S T acknowledge support of the Spanish MICINN Project SIP (PGC2018-101743-B-I00).

ORCID iDs

Sebin Varghese https://orcid.org/0000-0001-7204-7121
David Saleta Reig https://orcid.org/0000-0003-3189-2331
Alexander Block https://orcid.org/0000-0001-9288-5405
Alexandros El Sachat https://orcid.org/0000-0003-3798-9724
Marianna Sledzinska https://orcid.org/0000-0001-8592-1121

Clivia M Sotomayor Torres https://orcid.org/0000-0001-9986-2716
Klaas-Jan Tielrooij https://orcid.org/0000-0002-0055-6231

References

[1] Ando T 2006 Screening effect and impurity scattering in monolayer graphene *J. Phys. Soc. Japan* **75** 074716
[2] Adam S, Hwang E H and Das Sarma S 2008 Scattering mechanisms and Boltzmann transport in graphene *Physica* E **40** 1022–5
[3] Trolle M L, Pedersen T G and Véniard V 2017 Model dielectric function for 2D semiconductors including substrate screening *Sci. Rep.* **7** 39844
[4] Florian M, Hartmann M, Steinhoff A, Julian Klein A W, Finley J J, Wehling T O, Kaniber M and Gies C 2018 The dielectric impact of layer distances on exciton and trion binding energies in van der Waals heterostructures *Nano Lett.* **18** 2725–32
[5] Gabourie A J, Suryavanshi S V, Farimani A B and Pop E 2020 Reduced thermal conductivity of supported and encased monolayer and bilayer MoS_2 *2D Mater.* **8** 011001
[6] Qin-Yi Li, Xia K, Zhang J, Zhang Y, Li Q, Takahashi K and Zhang X 2017 Measurement of specific heat and thermal conductivity of supported and suspended graphene by a comprehensive Raman optothermal method *Nanoscale* **9** 10784–93
[7] Principi A, Lundeberg M B, Hesp N C H, Tielrooij K-J, Koppens F H L and Polini M 2017 Super-Planckian electron cooling in a van der Waals stack *Phys. Rev. Lett.* **118** 126804
[8] Bolotin K I, Sikes K J, Jiang Z, Klima M, Fudenberg G, Hone J, Kim P and Stormer H L 2008 Ultrahigh electron mobility in suspended graphene *Solid State Commun.* **146** 351–5
[9] Jin T, Kang J, Kim E S, Lee S and Lee C 2013 Suspended single-layer MoS_2 devices *J. Appl. Phys.* **114** 164509
[10] Nair R R, Blake P, Grigorenko A N, Novoselov K S, Booth T J, Stauber T, Peres N M R and Geim A K 2008 Fine structure constant defines visual transparency of graphene *Science* **320** 1308
[11] Yifei Y, Yiling Y, Chao X, Cai Y-Q, Liqin S, Zhang Y, Zhang Y-W, Gundogdu K and Cao L 2016 Engineering substrate interactions for high luminescence efficiency of transition-metal dichalcogenide monolayers *Adv. Funct. Mater.* **26** 4733–9
[12] Cai W, Moore A L, Zhu Y, Xuesong Li, Chen S, Shi Li and Ruoff R S 2010 Thermal transport in suspended and supported monolayer graphene grown by chemical vapor deposition *Nano Lett.* **10** 1645–51
[13] Morell N *et al* 2019 Optomechanical measurement of thermal transport in two-dimensional $MoSe_2$ lattices *Nano Lett.* **19** 3143–50
[14] Frank I W, Tanenbaum D M, van der Zande A M and McEuen P L 2007 Mechanical properties of suspended graphene sheets *J. Vac. Sci. Technol.* B **25** 2558–61
[15] Babacic V, Reig D S, Varghese S, Vasileiadis T, Coy E, Tielrooij K-J and Graczykowski B 2021 Thickness-dependent elastic softening of few-layer free-standing $MoSe_2$ *Adv. Mater.* **33** 2008614
[16] Chaste J, Eichler A, Moser J, Ceballos G, Rurali R and Bachtold A 2012 A nanomechanical mass sensor with yoctogram resolution *Nat. Nanotechnol.* **7** 301–4
[17] Song X, Oksanen M, Sillanpää M A, Craighead H G, Parpia J M and Hakonen P J 2012 Stamp transferred suspended graphene mechanical resonators for radio frequency electrical readout *Nano Lett.* **12** 198–202
[18] Rickhaus P, Maurand R, Liu M-H, Weiss M, Richter K and Schönenberger C 2013 Ballistic interferences in suspended graphene *Nat. Commun.* **4** 2342
[19] Qiang X, Meng-Yue W, Schneider G F, Houben L, Malladi S K, Dekker C, Yucelen E, Dunin-Borkowski R E and Zandbergen H W 2013 Controllable atomic scale patterning of freestanding monolayer graphene at elevated temperature *ACS Nano* **7** 1566–72
[20] Bae J J, Jeong H Y, Han G H, Kim J, Kim H, Kim M S, Moon B H, Lim S C and Lee Y H 2017 Thickness-dependent in-plane thermal conductivity of suspended MoS_2 grown by chemical vapor deposition *Nanoscale* **9** 2541–7
[21] Pudasaini P R *et al* 2018 High-performance multilayer WSe_2 field-effect transistors with carrier type control *Nano Res.* **11** 722–30
[22] Azizi A *et al* 2015 Freestanding van der Waals heterostructures of graphene and transition metal dichalcogenides *ACS Nano* **9** 4882–90
[23] Argentero G *et al* 2017 Unraveling the 3D atomic structure of a suspended graphene/hBN van der Waals heterostructure *Nano Lett.* **17** 1409–16
[24] Castellanos-Gomez A, Buscema M, Molenaar R, Singh V, Janssen L, Herre S J Van D Z and Steele G A 2014 Deterministic transfer of two-dimensional materials by all-dry viscoelastic stamping *2D Mater.* **1** 011002
[25] Desai S B *et al* 2016 Gold-mediated exfoliation of ultralarge optoelectronically-perfect monolayers *Adv. Mater.* **28** 4053–8
[26] Frisenda R, Navarro-Moratalla E, Gant P, Pérez De Lara D, Jarillo-Herrero P, Gorbachev R V and Castellanos-Gomez A 2018 Recent progress in the assembly of nanodevices and Van der Waals heterostructures by deterministic placement of 2D materials *Chem. Soc. Rev.* **47** 53–68
[27] Brennan C J, Nguyen J, Yu E T and Lu N 2015 Interface adhesion between 2D materials and elastomers measured by buckle delaminations *Adv. Mater. Interfaces* **2** 1500176
[28] Torres J, Zhu Y, Liu P, Lim S C and Yun M 2018 Adhesion energies of 2D graphene and MoS_2 to silicon and metal substrates *Phys. Status Solidi* a **215** 1700512
[29] Shaw J C, Zhou H, Chen Y, Weiss N O, Liu Y, Huang Y and Duan X 2014 Chemical vapor deposition growth of monolayer $MoSe_2$ nanosheets *Nano Res.* **7** 511–7
[30] Tonndorf P *et al* 2013 Photoluminescence emission and Raman response of monolayer MoS_2, $MoSe_2$ and WSe_2 *Opt. Express* **21** 4908–16
[31] Zhang Y *et al* 2014 Direct observation of the transition from indirect to direct bandgap in atomically thin epitaxial $MoSe_2$ *Nat. Nanotechnol.* **9** 111–5
[32] Sun Y, Wang D and Shuai Z 2016 Indirect-to-direct band gap crossover in few-layer transition metal dichalcogenides: a theoretical prediction *J. Phys. Chem.* C **120** 21866–70
[33] Chen Z, Liu H, Chen X, Chu G, Chu S and Zhang H 2016 Wafer-size and single-crystal $MoSe_2$ atomically thin films grown on GaN substrate for light emission and harvesting *ACS Appl. Mater. Interfaces* **8** 20267–73
[34] Cartamil-Bueno S J, Cavalieri M, Wang R, Houri S, Hofmann S and van der Zant H S J 2017 Mechanical characterization and cleaning of CVD single-layer h-BN resonators *npj 2D Mater. Appl.* **1** 16
[35] Palacios-Berraquero C, Kara D M, Alejandro R-P Montblanch M B, Latawiec P, Duhee Yoon A K Ott M L, Ferrari A C and Atatüre M 2017 Large-scale quantum-emitter arrays in atomically thin semiconductors *Nat. Commun.* **8** 15093
[36] Wang Y Y *et al* 2016 Determination of the thickness of two-dimensional transition-metal dichalcogenide by the Raman intensity of the substrate *Mater. Res. Express* **3** 025007

[37] Xiao-Li Li, Han W-P, Jiang-Bin W, Qiao X-F, Zhang J and Tan P-H 2017 Layer-number dependent optical properties of 2D materials and their application for thickness determination *Adv. Funct. Mater.* **27** 1604468
[38] Castellanos-Gomez A, Roldán R, Cappelluti E, Buscema M, Guinea F, van der Zant H S J and Steele G A 2013 Local strain engineering in atomically thin MoS_2 *Nano Lett.* **13** 5361–6
[39] Tongay S, Zhou J, Ataca C, Kelvin L, Matthews T S, Jingbo Li, Grossman J C and Junqiao W 2012 Thermally driven crossover from indirect toward direct bandgap in 2D semiconductors: $MoSe_2$ versus MoS_2 *Nano Lett.* **12** 5576–80
[40] Larentis S, Fallahazad B and Tutuc E 2012 Field-effect transistors and intrinsic mobility in ultra-thin $MoSe_2$ layers *Appl. Phys. Lett.* **101** 223104
[41] Horzum S, Sahin H, Cahangirov S, Cudazzo P, Rubio A, Serin T and Peeters F M 2013 Phonon softening and direct to indirect band gap crossover in strained single-layer $MoSe_2$ *Phys. Rev.* B **87** 125415
[42] Niu Y *et al* 2018 Thickness-dependent differential reflectance spectra of monolayer and few-layer MoS_2, $MoSe_2$, WS_2 and WSe_2 *Nanomaterials* **8** 725
[43] Zhang X, Sun D, Yilei Li, Lee G-H, Cui X, Chenet D, You Y, Heinz T F and Hone J C 2015 Measurement of lateral and interfacial thermal conductivity of single-and bilayer MoS_2 and $MoSe_2$ using refined optothermal Raman technique *ACS Appl. Mater. Interfaces* **7** 25923–9
[44] Beal A R, Knights J C and Liang W Y 1972 Transmission spectra of some transition metal dichalcogenides. II. Group VIA: trigonal prismatic coordination *J. Phys.* C **5** 3540
[45] Bromley R A, Murray R B and Yoffe A D 1972 The band structures of some transition metal dichalcogenides. III. Group VIA: trigonal prism materials *J. Phys.* C **5** 759
[46] Dong N, Yuanxin Li, Feng Y, Zhang S, Zhang X, Chang C, Fan J, Zhang L and Wang J 2015 Optical limiting and theoretical modelling of layered transition metal dichalcogenide nanosheets *Sci. Rep.* **5** 14646
[47] Zhao W, Ghorannevis Z, Chu L, Toh M, Kloc C, Tan P-H and Eda G 2013 Evolution of electronic structure in atomically thin sheets of WS_2 and WSe_2 *ACS Nano* **7** 791–7
[48] Frisenda R, *et al* 2017 Micro-reflectance and transmittance spectroscopy: a versatile and powerful tool to characterize 2D materials *J. Phys.* D **50** 074002
[49] Jin W *et al* 2015 Substrate interactions with suspended and supported monolayer MoS_2: angle-resolved photoemission spectroscopy *Phys. Rev.* B **91** 121409
[50] Rusen Yan J R Simpson S B, Brivio J, Watson M, Xufei W, Kis A, Tengfei Luo A R Walker H and Xing H G 2014 Thermal conductivity of monolayer molybdenum disulfide obtained from temperature-dependent Raman spectroscopy *ACS Nano* **8** 986–93
[51] Dai Z, Jin W, Grady M Sadowski J T, Dadap J I, Osgood Jr R M and Pohl K 2017 Surface structure of bulk 2H-MoS_2 (0001) and exfoliated suspended monolayer MoS_2: a selected area low energy electron diffraction study *Surf. Sci.* **660** 16–21
[52] Bertolazzi S, Brivio J and Kis A 2011 Stretching and breaking of ultrathin MoS_2 *ACS Nano* **5** 9703–9
[53] Huang X *et al* 2021 Raman spectra evidence for the covalent-like quasi-bonding between exfoliated MoS_2 and au films *Sci. China Information Sci.* **64** 1–9
[54] Morell N, Reserbat-Plantey A, Tsioutsios I, Schädler K G, Dubin F, Koppens F H L and Bachtold, A 2016 High quality factor mechanical resonators based on WSe_2 monolayers *Nano Lett.* **16** 5102–8
[55] Easy E, Gao Y, Wang Y, Yan D, Goushehgir S M, Yang E-H, Xu B and Zhang X 2021 Experimental and computational investigation of layer-dependent thermal conductivities and interfacial thermal conductance of one-to three-layer WSe_2 *ACS Appl. Mater. Interfaces* **13** 13063–71
[56] Viana B C *et al* 2020 Temperature-and power-dependent phonon properties of suspended few layers of tungsten diselenide *Vib. Spectrosc.* **111** 103169
[57] Zhang R, Koutsos V and Cheung R 2016 Elastic properties of suspended multilayer WSe_2 *Appl. Phys. Lett.* **108** 042104
[58] Zobeiri H, Wang R, Zhang Q, Zhu G and Wang X 2019 Hot carrier transfer and phonon transport in suspended nm WS_2 films *Acta Mater.* **175** 222–37
[59] Zobeiri H, Wang R, Wang T, Lin H, Deng C and Wang X 2019 Frequency-domain energy transport state-resolved Raman for measuring the thermal conductivity of suspended nm-thick $MoSe_2$ *Int. J. Heat Mass Transfer* **133** 1074–85
[60] Wang R, Wang T, Zobeiri H, Yuan P, Deng C, Yue Y, Shen X and Wang X 2018 Measurement of the thermal conductivities of suspended MoS_2 and $MoSe_2$ by nanosecond ET-Raman without temperature calibration and laser absorption evaluation *Nanoscale* **10** 23087–102